(14) S. Nomura, A. Asanuma, S. Suehiro, and H. Kawai, *J. Polym. Sci., Part A-2*, **9**, 1991 (1971).
(15) S. Nomura, M. Matsuo, and H. Kawai, *J. Polym. Sci., Polym. Phys. Ed.*, **10**, 2489 (1972).
(16) M. Matsuo, H. Hattori, S. Nomura, and H. Kawai, *J. Polym. Sci., Polym. Phys. Ed.*, **14**, 223 (1976).
(17) Z. W. Wilchinsky, *J. Appl. Phys.*, **30**, 792 (1959).
(18) Z. W. Wilchinsky, *J. Appl. Phys.*, **31**, 1969 (1960).
(19) R. A. Sack, *J. Polym. Sci.*, **54**, 543 (1961).
(20) P. Erhardt and R. S. Stein, *J. Polym. Sci., Part B*, **3**, 553 (1965).
(21) R. S. Stein, T. Tanaka, E. Chang, and I. Kimura, ONR Technical Report No. 111, Polymer Research Institute, University of Massachusetts, Amherst, Mass., August 1968.
(22) T. Hashimoto, O. J. Phillips, and R. S. Stein, paper presented at the IUPAC Meeting, Leiden, The Netherlands, September 1970.
(23) T. Oda and R. S. Stein, *J. Polym. Sci., Part A-2*, **10**, 685 (1972).
(24) T. Hashimoto, H. Kawai, and R. S. Stein, paper presented at the 19th Symposium on Rheorogy, Japan, Nagoya, October 1971.
(25) R. J. Roe and W. R. Krigbaum, *J. Chem. Phys.*, **40**, 2608 (1964).
(26) W. R. Krigbaum and R. J. Roe, *J. Chem. Phys.*, **41**, 737 (1964).
(27) R. J. Roe, *J. Appl. Phys.*, **36**, 2024 (1965).
(28) W. R. Krigbaum and Y. I. Balta, *J. Phys. Chem.*, **71**, 1770 (1967).
(29) W. R. Krigbaum, T. Adachi, and J. V. Dawkins, *J. Chem. Phys.*, **49**, 1532 (1968).
(30) W. Spendly, G. R. Hext, and F. R. Himsworth, *Technometrics*, **4**, 441 (1962).
(31) J. A. Nelder and R. Mead, *Comput. J.*, **7**, 308 (1965).
(32) R. S. Stein and F. H. Norris, *J. Polym. Sci.*, **21**, 381 (1956).
(33) H. Takahara, S. Nomura, H. Kawai, Y. Yamaguchi, K. Okazaki, and A. Fukushima, *J. Polym. Sci., Part A-2*, **6**, 197 (1968).
(34) D. Y. Yoon, C. Chang, and R. S. Stein, *J. Polym. Sci., Polym. Phys. Ed.*, **12**, 2091 (1974).
(35) J. J. van Aartsen and R. S. Stein, *J. Polym. Sci., Part A-2*, **9**, 295 (1971).
(36) T. T. Wang, *J. Appl. Phys.*, **44**, 4052 (1973).
(37) T. T. Wang, *J. Polym. Sci., Polym. Phys.* Ed., **12**, 445 (1974).
(38) M. Matsuo, T. Ogita, S. Suehiro, T. Yamada, and H. Kawai *Macromolecules*, **11**, 521 (1978).

Effects of Casting Solvents on Mechanical and Structural Properties of Polydiene-Hydrogenated Polystyrene–Polyisoprene–Polystyrene and Polystyrene–Polybutadiene–Polystyrene Block Copolymers

R. Séguéla and J. Prud'homme*

Department of Chemistry, University of Montreal, Montreal Quebec, Canada H3C 3VI. *Received May 1, 1978*

ABSTRACT: Stress–strain and dynamic mechanical measurements were carried out over a range of temperatures for a polyisoprene-hydrogenated SIS block copolymer and for a polybutadiene-hydrogenated SBS block copolymer having polystyrene endblocks of about the same molecular weights close to 1×10^4 and having styrene weight fractions of 0.22 and 0.29, respectively. Specimens were prepared by solvent casting from solutions in heptane, cyclohexane, and toluene. Microdomain structures were investigated by small-angle X-ray scattering. Depending upon the casting solvent, the hydrogenated SIS copolymer exhibited spherical or cylindrical polystyrene structures while the hydrogenated SBS copolymer exhibited spherical, cylindrical, or lamellar polystyrene structures. The three structures were obtained in the order of increasing solvent affinity for polystyrene. The mechanical behavior of the specimens with spherical microdomains was very close to those of unfilled vulcanized rubbers. In contrast, specimens with cylindrical structures showed stress softening on repeated extensions and those with lamellar structures showed yield and neck propagation in the first extension. The systematic change of microdomain structure with increasing solvent affinity for polystyrene is interpreted in terms of solvent partition within the micellar arrangement produced during the casting process. Also discussed are the relations between domain sizes and unperturbed chain dimensions for the three types of structures observed.

In a previous paper[1] we reported physical and mechanical properties of a polyisoprene-hydrogenated polystyrene–polyisoprene–polystyrene (SIS) elastomeric block copolymer containing 22% by weight of styrene. The copolymer showed two glass transitions at −67 and ~90 °C, respectively, and its stress–strain curves measured at room temperature in successive extension cycles ($0 < \epsilon \leq 3$) were nearly reversible and superposable, indicating a microphase system in which the polystyrene cross-linking domains were discrete and particularly well isolated. In contrast, the original SIS copolymer showed irreversible stress softening in the first extension cycle. Both specimens were prepared by solution casting at room temperature using cyclohexane as solvent. Cyclohexane is a poor solvent for polystyrene and a good solvent for both polyisoprene and hydrogenated polyisoprene. As will be shown in the present paper, we also have observed that a polybutadiene-hydrogenated SBS block copolymer containing 29% by weight of styrene does not exhibit the stress-softening effect when cast from heptane, a non-solvent for polystyrene but a good solvent for hydrogenated polybutadiene.

Solution casting from preferential solvents for polydienes is known[2-5] to improve the rubber-like behavior of SIS and SBS block copolymers having a styrene content in the range of 15 to 30% by weight. Such solvents swell preferentially the polydiene phase and thereby give rise to a better dispersion of the polystyrene phase which after complete solidification of the material appears as discrete glassy domains in a continuous rubbery matrix. However, it has been observed[2,6] that SIS and SBS films cast from preferential solvent for the polydienes exhibit stress softening on repeated extensions. This phenomenon was attributed to irreversible processes such as rupture of interconnections between some of the glassy domains or deformation of the latter. It is similar to the Mullins effect in reinforced rubbers. The stress-softening phenomenon also occurs for compression molded or extruded specimens[2,7-9] but, as shown by Pedemonte et al.,[9] it disappears when such specimens are swollen with a

0024-9297/78/2211-1007$01.00/0

preferential solvent for the polydiene and are subsequently dried under vacuum.

In view of the particular behavior of the hydrogenated SIS and SBS block copolymers which do not exhibit a marked stress-softening effect when cast from cyclohexane and heptane, respectively, it was decided to investigate in more detail the effect of casting solvent on the mechanical properties of these copolymers. For that purpose, films cast from heptane, cyclohexane, and toluene were studied. The latter is a good solvent for both polystyrene and the hydrogenated polydienes. In the present paper we report the results of this investigation. The mechanical measurements were carried out over a range of temperatures. They are discussed in terms of the microphase structure. Information concerning domain morphologies has been obtained by means of small-angle X-ray scattering.

Experimental Section

Materials and Molecular Characterizations. Preparation and characterization of the polyisoprene-hydrogenated SIS block copolymer have been described in a previous paper.[1] The polybutadiene-hydrogenated SBS block copolymer was a commercial polymer manufactured by Shell Chemical Co. under the trade name Kraton GX-6500. Number-average molecular weights were determined in toluene at 25 °C using a Mechrolab 503 Rapid Osmometer with Schleicher and Schuell 08 grade membrane filters. Styrene contents and midblock microstructures were determined by 220-MHz NMR analysis using carbon tetrachloride as the solvent. Gel-permeation chromatography measurements were performed at 35 °C with a Water Associates Model 200 instrument. A series arrangement of four Waters styragel columns with upper porosity designations 10^6, 10^5, 10^4, and 10^3 Å was used. The mobile phase was reagent-grade toluene and its flow rate was 1 mL/min. A 2-mL portion of solution, 5×10^{-3} g/cm^3 concentration, was injected.

Film Preparation. Film specimens about 0.5 mm thick were prepared by casting the polymers from 5% solutions on mercury. In each case the solvent was slowly evaporated at room temperature for a period of 3 to 4 days and the cast films were subsequently dried under high vacuum for 1 week. The solvents were filtered and dried reagent-grade toluene, cyclohexane, and heptane.

Physical Measurements. Density measurements were made at 25 °C using a water–methanol density gradient column calibrated with glass beads of known density. Glass transitions and crystallization phenomena were studied with a Perkin-Elmer Differential Scanning Calorimeter Model DSC-IB.

Mechanical Measurements. Stress–strain curves were measured using an Instron Tensile Tester Model 1130. An environmental chamber was used to obtain data at constant temperature over the temperature range of −60 to 80 °C. Test pieces were 5 cm in length and 0.5 cm in width. A crosshead speed of 4 cm/min was used. Dynamic tensile mechanical measurements were made using a Rheovibron Dynamic Viscoelastometer Model DDV-II. Test pieces were about 1–2 cm in length and 0.5 cm in width. The measurements were carried out over the temperature range −140 to 160 °C at average intervals of 3 °C. Data were corrected for apparatus compliance using an empirical correction factor measured at near zero length as a function of temperature.

Small-Angle X-ray Scattering. Small-angle X-ray scattering photographs were taken with a Rigaku-Denki Goniometer Model 2202. Cu Kα radiation (λ 1.54 Å) was generated by a Philips tube operated at 40 kV and 20 mA. The primary beam, filtered with a nickel foil, was collimated by means of two pinholes. The second pinhole, specimen, and photographic films were placed at 300, 320, and 600 mm from the first pinhole, respectively. The diameters of the first and second pinholes were 0.5 and 0.3 mm, respectively.

Results

Molecular weights, styrene contents, and densities of the two samples studied in the present work are summarized in Table I. The polyisoprene midblock of the SIS copolymer which was hydrogenated had the following microstructure:[1] 71% *cis*-1,4, 22% *trans*-1,4, and 7% 3,4. NMR analysis of the hydrogenated sample, designated as SIS-6-H in Table I, showed quantitative saturation of the isoprene units.[1] Thus the elastomeric midblock of this polymer is essentially an alternating copolymer of ethylene and propylene with 3.5 mol % of 2-isopropyl-1-butene units. On the other hand, NMR analysis of the Kraton GX-6500 sample indicated that the rubber midblock of this polymer was a random copolymer of ethylene and 1-butene having an ethylene molar content close to 78%. As shown in Figure 1, the GPC curves of the two copolymer samples, SIS-6-H and Kraton-G, indicate unimodal molecular weight distributions and low polydispersities. For the sake of comparison, the GPC curve of a Waters polystyrene standard of known polydispersity also is included in Figure 1.

Table I
Molecular Weights, Styrene Contents, and Densities of the Material Samples Studied in the Present Work

sample	$\bar{M}_n \times 10^{-5}$	w_S[a]	ρ^{25}, g cm^{-3}
SIS-6-H	1.17	0.22	0.891
Kraton GX-6500	0.69	0.29	0.907

[a] Weight fraction of styrene calculated from 200-MHz NMR spectra.

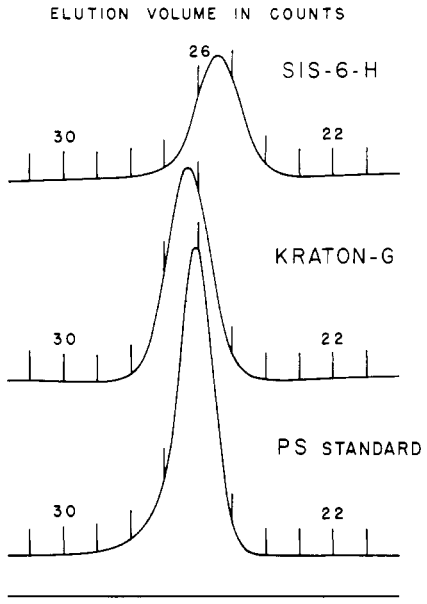

Figure 1. GPC elution curves for sample SIS-6-H, Kraton-G, and a polystyrene standard ($\bar{M}_n = 1.10 \times 10^5$, $\bar{M}_w/\bar{M}_n = 1.02$).

1. Thermomechanical Behavior. (a) Stress–Strain Properties. Figure 2a and 2b show stress–strain curves measured on SIS-6-H copolymer specimens cast from cyclohexane and toluene, respectively. The measurements were carried out at 25 °C. In each case the specimen was submitted to two consecutive extension cycles to a strain $\epsilon = 3$ which corresponds to approximately half the elongation at break for the cyclohexane cast film. The specimen was relaxed for 10 min between the first and second cycle. As can be seen from Figure 2a, the mechanical behavior of cyclohexane cast film is very similar to that of unfilled cross-linked rubber. The two consecutive cycles are nearly reversible and superposable. In contrast, as can be seen from Figure 2b, sample cast from toluene exhibits marked stress softening in the first extension cycle, indicating a filler effect for this material.

The difference between the mechanical behavior of the two specimens is more evident in Figure 3 where their nominal tensile stresses measured on first extension at ϵ

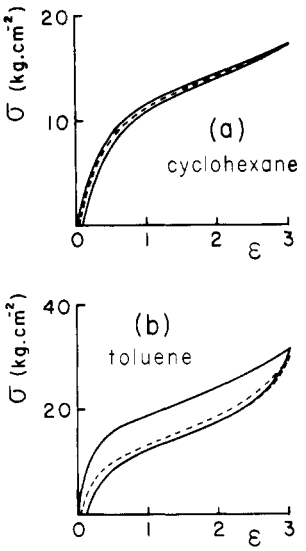

Figure 2. Stress–strain curves for SIS-6-H films cast from cyclohexane (a) and toluene (b): first cycle (—), second cycle (---).

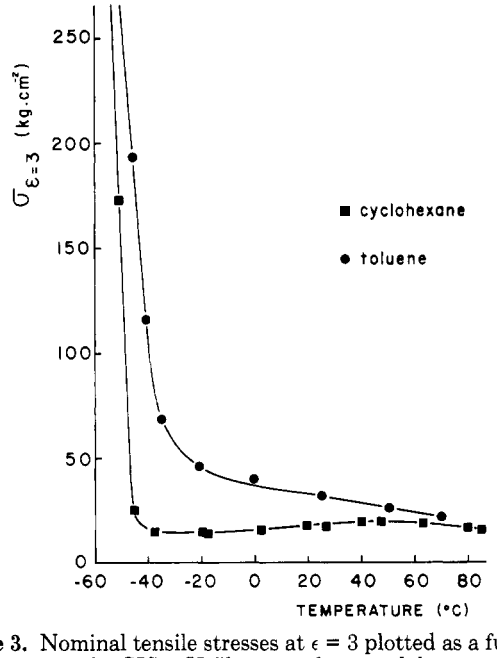

Figure 3. Nominal tensile stresses at $\epsilon = 3$ plotted as a function of temperature for SIS-6-H films cast from cyclohexane (■) and toluene (●).

= 3 are plotted as a function of temperature between −60 and 80 °C. Figure 3 shows that nominal tensile stress of the cyclohexane cast film is nearly constant between 80 and −45 °C where it increases sharply owing to the vitrification of the elastomeric phase. In contrast, nominal tensile stress of the toluene cast film increases gradually with decreasing temperature and shows a glass transition phenomenon at about −40 °C. A more detailed inspection of the rubbery plateau observed for the cyclohexane cast film reveals a slight decrease in tensile stress with decreasing temperature between 40 and −20 °C. Interestingly, in this range of temperature, nominal stress variation is nearly proportional to the product of temperature with density, $T\rho$, as predicted from the rubber elasticity theory.[10] Note that above 50 °C, tensile stress decreases slightly with increasing temperature owing to the softening of the polystyrene microdomains.

Figure 4a, 4b, and 4c show the 25 °C stress–strain curves measured on Kraton-G specimens cast from heptane, cyclohexane, and toluene, respectively. Figure 4a shows

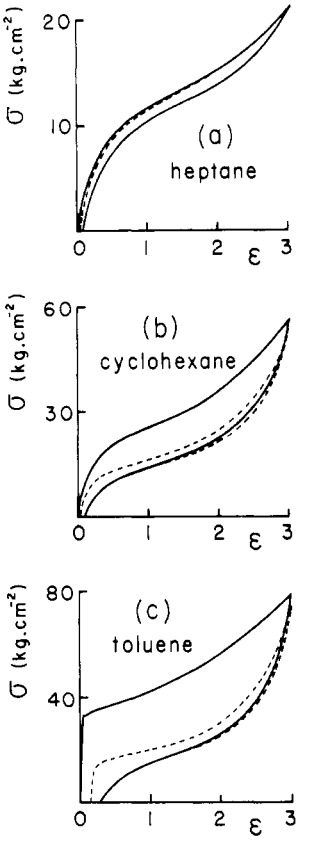

Figure 4. Stress–strain curves for Kraton-G films cast from heptane (a), cyclohexane (b), and toluene (c): first cycle (—), second cycle (---).

that Kraton-G film cast from heptane, a nonsolvent for polystyrene, does not exhibit significant stress softening in the first extension cycle while Figure 4b shows that the specimen cast from cyclohexane exhibits stress softening. In fact, the latter specimen behaves more like the SIS-6-H specimen cast from toluene. On the other hand, as shown in Figure 4c, the stress–strain curve measured on Kraton-G film cast from toluene exhibits a yield at low elongation indicating plastic deformation caused by the breakdown of a continuous polystyrene microphase. The behavior differences observed between SIS-6-H and Kraton-G films cast from either cyclohexane or toluene are presumably caused by the higher styrene content in Kraton-G.

Figure 5 shows the nominal tensile stresses measured at $\epsilon = 3$ plotted as a function of temperature for the three Kraton-G specimens. Here again, one can observe that the film which did not exhibit significant stress softening in the first extension cycle, namely the specimen cast from heptane, presents a nearly constant tensile stress between 70 and −10 °C. In contrast, the specimens cast from either cyclohexane or toluene show a continuous increase of tensile stress with decreasing temperature.

In the case of heptane cast film, inspection of Figure 5 reveals that the transition from the rubbery plateau to the high tensile zone is not as sharp for this specimen as that observed for SIS-6-H film cast from cyclohexane (Figure 3). It is also interesting to note that the transition appears at −20 °C for Kraton-G, a temperature which is 25 °C higher than that observed in Figure 3 for the SIS-6-H copolymer. This difference is not associated with a higher glass transition of the rubbery phase in Kraton-G but arises from the crystallization of the 78 mol % ethylene milblock. This is demonstrated in Figure 6 which shows both DSC heating and cooling curves measured on the Kraton-G specimen cast from heptane. Both curves were measured

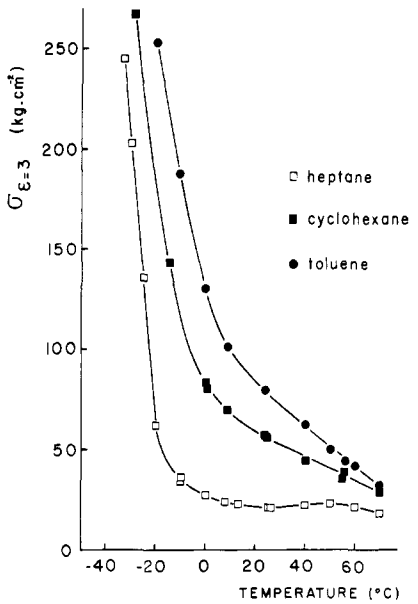

Figure 5. Nominal tensile stresses at $\epsilon = 3$ plotted as a function of temperature for Kraton-G films cast from heptane (□), cyclohexane (■), and toluene (•).

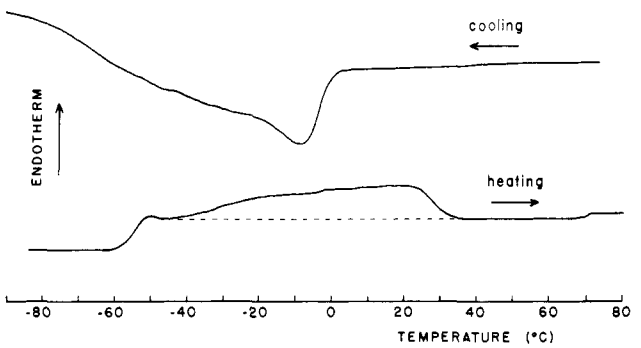

Figure 6. DSC heating and cooling curves measured at 40 °C min^{-1} for a Kraton-G specimen cast from heptane.

at 40 °C min^{-1}. Before the heating curve measurement was made, the sample was heated to 100 °C and cooled to −100 °C at a rate of 5 °C min^{-1}. The heating curve shows a distinct glass transition near 60 °C followed by a diffuse melting peak in the −40 to 30 °C region. A less distinct polystyrene glass transition is observed near 70 °C. On the other hand, the cooling curve shows a sharp crystallization exotherm with a minimum at −10 °C. The same behavior was observed for Kraton-G specimens cast from both cyclohexane and toluene.

(b) Dynamic Viscoelastic Properties. Figures 7 and 8 show tan δ and storage modulus, E', measured as functions of temperature for SIS-6-H films cast from cyclohexane and toluene, respectively. The dynamic measurements were carried out at a frequency of 110 Hz. Comparison of Figures 7 and 8 reveals that the main differences between the two specimens are first a higher storage modulus for the toluene cast film in the temperature between the glass transitions of the two components, and second a greater polystyrene tan δ peak for this latter specimen. Note that the value of the storage modulus, E', in the rubbery plateau observed in Figure 7 for the cyclohexane cast specimen is about three orders of magnitude lower than that measured at low temperatures, when both components are glassy. This behavior is characteristic of an unfilled elastomer.[11] It indicates that in this range of temperatures the load is essentially carried by the elastomeric phase. In contrast, increase of storage

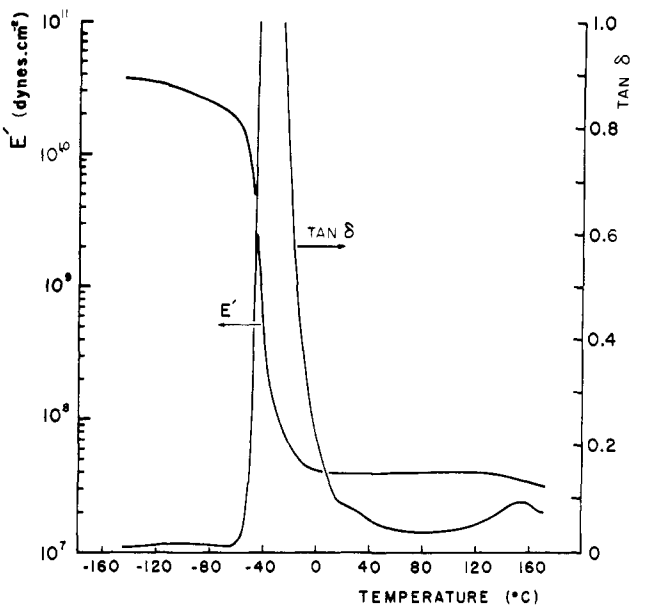

Figure 7. Dynamic storage modulus, E', and tan δ plotted as functions of temperature for SIS-6-H film cast from cyclohexane.

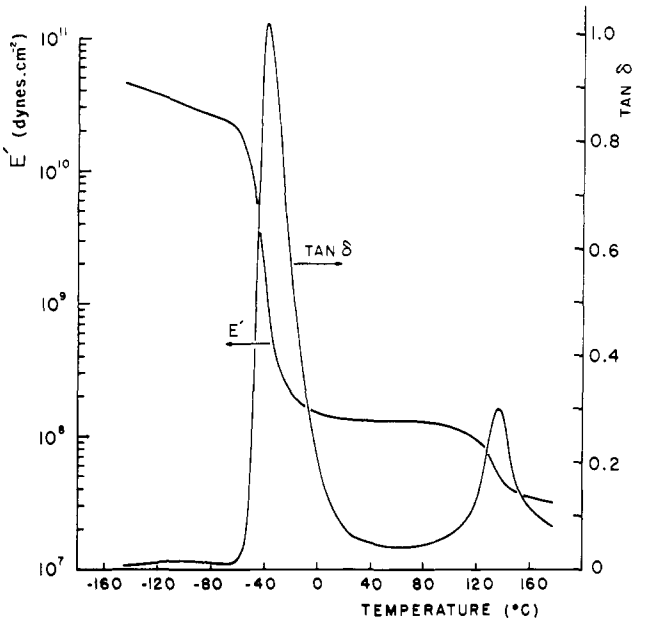

Figure 8. Dynamic storage modulus, E', and tan δ plotted as functions of temperature for SIS-6-H film cast from toluene.

modulus in the rubbery plateau as observed in Figure 8 for toluene cast film indicates that a fraction of the load is carried by either the polystyrene glassy phase or a nonelastomeric mixed phase. The fact that no significant intermediate transition is observed in the tan δ curve of Figure 8 suggests that there is no mixed phase in the toluene cast specimen. Thus both the increase of the rubbery storage modulus and the stress-softening effect observed previously for this specimen are likely to be caused by a microphase structure in which the polystyrene glassy domains are sufficiently extended in one direction to act as an active filler.

Figures 9 and 10 show storage modulus, E', and tan δ, respectively, measured as functions of temperature for Kraton-G films cast from heptane, cyclohexane, and toluene. As in the case of the SIS-6-H copolymer, both the storage modulus values in the rubbery plateau (Figure 9) and the respective heights of tan δ for the polystyrene and the elastomeric phases (Figure 10) indicate that the

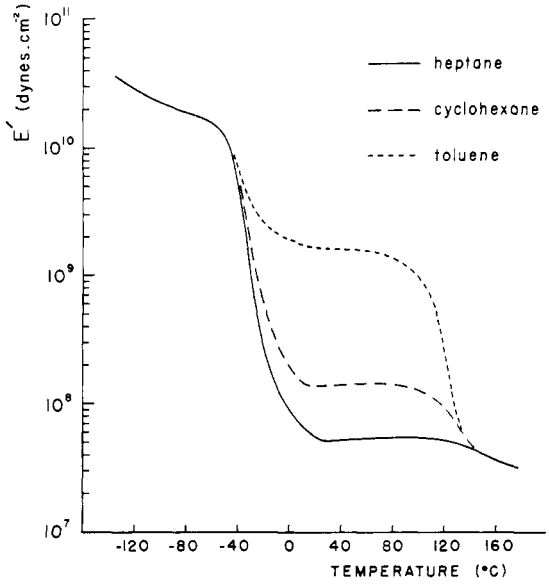

Figure 9. Dynamic storage modulus, E', plotted as a function of temperature for Kraton-G films cast from heptane (—), cyclohexane (– – –), and toluene (- - -).

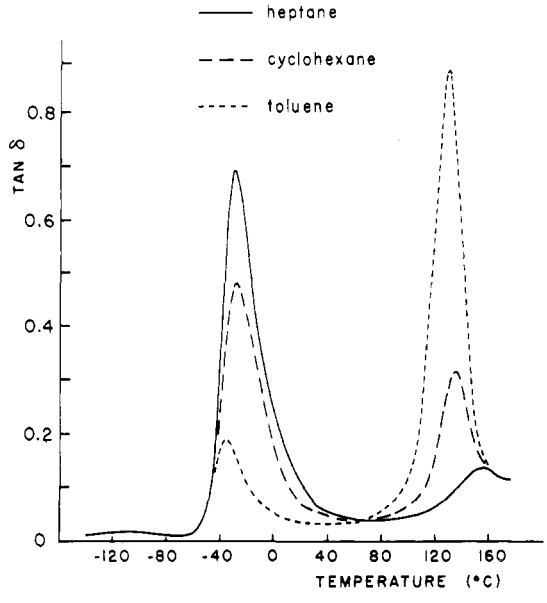

Figure 10. Tan δ plotted as a function of temperature for Kraton-G films cast from heptane (—), cyclohexane (– – –), and toluene (- - -).

load carried by the polystyrene phase increases in the following order: heptane < cyclohexane < toluene. One can also observe in Figure 9 that the heptane cast film gives an E' value in the rubbery region which is about three orders of magnitude lower than that measured when both components are glassy. This difference in E' becomes less important for the cyclohexane cast film, the behavior of which is essentially similar to that previously observed for the SIS-6-H specimen cast from toluene, and decreases to about one order of magnitude for the toluene cast film. It can also clearly be seen in Figure 10 that the position of the tan δ peak associated with the polystyrene phase is shifted to higher temperature in the order: toluene < cyclohexane < heptane. A similar effect also appeared in the case of SIS-6-H copolymer specimens (Figure 7 and 8). On the other hand, the position of the tan δ peak associated with the elastomeric phase in both SIS-6-H and Kraton-G films does not change markedly with the nature of the casting solvent. Only that of the Kraton-G specimen

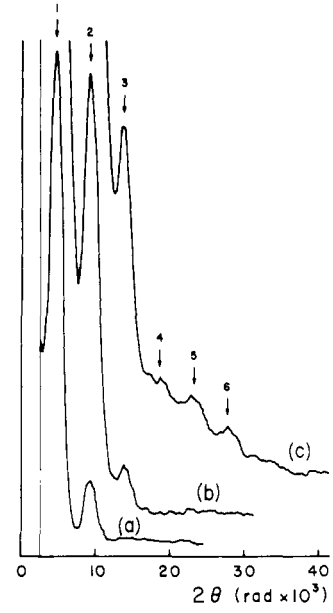

Figure 11. Small-angle X-ray scattering curve measured on a Kraton-G film cast from toluene. Exposure time: (a) 2 h, (b) 20 h, (c) 72 h. Arrows indicate the diffraction line positions calculated for a lamellar structure from the main peak Bragg spacing d_1 = 332 Å.

cast from toluene appears to be shifted slightly to lower temperature than those of the specimens cast from heptane and cyclohexane. Similar tan δ shifts have been observed by Kraus et al.[12] and more recently by Beamish et al.[5] for SBS block copolymers having styrene contents close to 30% by weight. The SBS films cast from good solvents for polystyrene but nonsolvents for polybutadiene showed polystyrene tan δ peaks shifted to lower temperatures than those of films cast from a good solvent for both the parent homopolymers. They also exhibited greater storage modulus, E', in the rubbery region. Obviously, this behavior is associated with a larger load carried by the polystyrene glassy microphase. For the SBS specimens studied by Kraus et al.,[12] this has been confirmed by electron micrographs in which the high modulus specimens presented long-range cylindrical or lamellar structures and the low modulus specimens presented randomly oriented short polystyrene rods.

Direct observations under an electron microscope of the microdomain morphologies in the specimens studied in the present work are difficult owing to the impossibility to achieve sufficient contrast between the two chemically different phases as it is usually done using the osmium tetroxide staining technique for either SBS or SIS materials. For that reason, the microdomain structures in the present specimens were investigated by small-angle X-ray scattering (SAXS).

2. SAXS Characterization of the Microdomain Structures. All the SAXS measurements were carried out using pinhole collimators and photographic films as the recording medium. The scattering intensities were read on the negatives by means of a Joyce-Loebl recording microdensitometer. The unstretched specimens of both SIS-6-H and Kraton-G materials prepared from the different solvents gave Debye–Scherrer circular diffraction patterns showing several maxima whose positions were solvent dependent.

Figures 11–13 show the scattering curves measured on Kraton-G films prepared from toluene, cyclohexane, and heptane, respectively. The first curve (Figure 11) exhibits six distinctive peaks while the other two curves (Figures 12 and 13) show only three peaks. In all cases the first

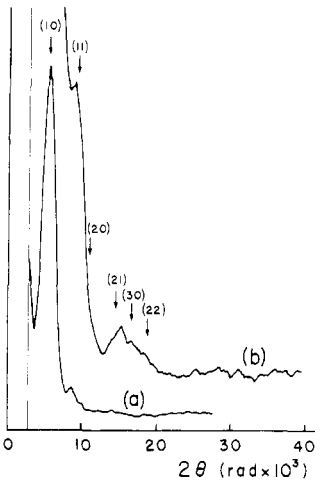

Figure 12. Small-angle X-ray scattering curve measured on a Kraton-G film cast from cyclohexane. Exposure time: (a) 2 h, (b) 48 h. Arrows indicate the diffraction line positions calculated from eq 1 for a two-dimensional lattice of hexagonally packed cylinders of unit cell dimension a = 327 Å.

Figure 13. Small-angle X-ray scattering curve measured on a Kraton-G film cast from heptane. Exposure time: (a) 3 h, (b) 72 h.

peak is by far the most intense. For the present measurements, the film surface was perpendicular to the incident beam. Other measurements with the film surface parallel to the incident beam have led to similar diffraction patterns indicating no preferential orientation of the microphase domains. The peak positions, 2θ, and their Bragg spacings, $\lambda/2 \sin \theta$, are given in Table II for the three specimens.

For the Kraton-G specimen cast from toluene, the Bragg spacings obtained correspond to the first six orders of diffraction expected for a lamellar structure,[13] i.e., $d_n = nd_1$ where d_1 is the first order spacing and n = 2, 3, 4, 5, and 6. The position of the expected difraction lines calculated from the main peak Bragg spacing, d_1 = 332 Å, are shown on Figure 11. Note that the fourth order is not as intense as the fifth and the sixth orders. According to Skoulios,[13] the fourth order should be absent for a lamellar structure in which the volume fraction of one of the two phases is $^1/_4$. This value is exactly that of the polystyrene volume fraction, ϕ_{PS}, one can estimate for the present block copolymer assuming its composition is w_S = 0.29, and its density is ρ = 0.907 g cm^{-3}, and the density of polystyrene is ρ_{PS} = 1.052. According to the Bragg spacings given in Table II, the separation between two consecutive

Table II
SAXS Peak Positions and Bragg Spacings for Kraton-G Specimens Cast from Toluene, Cyclohexane, and Heptane

casting solvent	peak position 2θ, rad × 10^3	Bragg spacing, Å
toluene	4.64	332
	9.20	167
	13.6	113
	18.7	82
	22.7	68
	27.5	56
cyclohexane	5.44	283
	8.75	176
	15.0	103
heptane	6.61	233
	13.8	112
	23.6	65

polystyrene lamellae should be close to 249 Å and the thickness of the individual polystyrene lamellae 83 Å.

For the Kraton-G specimen cast from cyclohexane, the Bragg spacings obtained are close to those one can expect for a two-dimensional lattice of hexagonally packed cylinders,[14] i.e.

$$d_{hk} = (3^{1/2}a/2)/(h^2 + hk + k^2)^{1/2} = \lambda/2 \sin \theta \quad (1)$$

where h and k are the Miller indices and a is the interaxial distance or the unit cell dimension in the hexagonal lattice. As shown on Figure 12, a good agreement is obtained between the experimental peak positions and the diffraction lines calculated by means of eq 1 if one attributes the first peak to the d_{10} order diffraction. This assignment leads to an interaxial distance a = 327 Å. However, the d_{20} order diffraction is not observable in Figure 15. A similar result was obtained by Lewis and Price[15] for a SBS compression molded specimen ($\bar{M}_n = 8.4 \times 10^4$, w_S = 0.26). They attributed the absence of the d_{20} order to the influence of the particle scattering factor $F(hR)$ ($h = (4\pi/\lambda) \sin \theta$, R = radius of the cylinders) which modulates the interparticle interference function.[14] From the polystyrene volume fraction ϕ_{PS} = 0.25 of the present polymer and from the interaxial distance a = 327 Å we obtain for the radius of the cylinders R = 86 Å. Note that the particle scattering factor for independent solid cylinders is[14]

$$F(hR) = 2J_1(hR)/hR \quad (2)$$

where J_1 is the Bessel function of first order. This function $F(hR)$ shows a first minimum at hR = 3.8 which, for a cylinder of radius R = 86 Å, corresponds to $2\theta = 10.8 \times 10^{-3}$ rad. This angle is exactly that expected for the d_{20} order diffraction peak of the present system.

The diffraction curve measured on Kraton-G film cast from heptane (Figure 13) shows three peaks among which only the first one (the most intense) can be attributed to interparticle interferences. This is demonstrated by Figure 14 where the diffraction curve of the same specimen stretched at ϵ = 1 is shown. The intensity was measured in the same direction as the extension direction. The curve demonstrates a shift of the first peak from $2\theta = 6.6 \times 10^{-3}$ rad in the unstretched state to $2\theta = 3.2 \times 10^{-3}$ rad and the apparition of a new diffraction peak at $2\theta = 5.5 \times 10^{-3}$ rad. The peaks at $2\theta = 13.8 \times 10^{-3}$ and 23.6×10^{-3} rad in the unstretched state did not shift, indicating that they arise from particle scattering. Interestingly, this behavior is similar to that observed by Inoue et al.[16] for a SI two-block copolymer ($\bar{M}_n = 2.78 \times 10^5$, w_S = 0.185) cast from toluene. Electron micrographs of the SI specimen showed spheres of polystyrene dispersed in a matrix of polyisoprene. This suggests that the microdomain structure of the Kraton-G

Figure 14. Small-angle X-ray scattering curve measured on a Kraton-G film cast from heptane, stretched at $\epsilon = 1$. Intensity measured in the same direction as the extension direction. Exposure time: (a) 5 h, (b) 48 h.

specimen cast from heptane is also characterized as discrete spheres of polystyrene dispersed in a rubbery matrix.

As proposed by Campos-Lopez et al.,[17] block copolymer structures having spherical domains may be considered as short-range ordered liquid-like structures. Oster and Riley[18] had previously shown that such ordered liquid-like structures should give rise to a main diffraction peak at a position which, using Bragg's law, should lead to a Bragg spacing close to the interparticle distance. If one assumes that is the case for the present system, the shift of the main peak to a smaller scattering angle upon stretching would be a measure of the change in interdomain distance along the stretching direction. The value of the Bragg spacing calculated from the position of the main peak observed for the unstretched specimen is 233 Å (Table II) while that calculated for the stretched ($\epsilon = 1$) specimen is 479 Å. These results suggest that a nearly affine deformation occurs in the stretched specimen. Another point which deserves mention is related to the fact that there is no change in the position of the second and third peaks upon stretching. As pointed out by Inoue et al.,[16] this would indicate that there is no deformation of the polystyrene microdomains from spherical to ellipsoidal morphology, for example.

Analysis of the second and third peak observed in Figure 13 using the Rayleigh equation for scattering by independent spheres[16,19] leads to the value $R = 98 \pm 4$ Å for the radius of the isolated polystyrene particles in the Kraton-G specimen cast from heptane. Interestingly, this value is close to the value $R = 91$ Å one can calculate from the polystyrene volume fraction, $\phi_{PS} = 0.25$, assuming a simple cubic arrangement.

In the case of the SIS-6-H materials cast from toluene and cyclohexane, SAXS studies confirm that their microdomain structures are essentially identical to those of the Kraton-G specimens cast from cyclohexane and heptane, respectively. This is shown in Figure 15 for the SIS-6-H specimen cast from toluene and in Figure 16 for the specimen cast from cyclohexane. In the first case (Figure 15), the scattering intensity curve shows peaks and shoulders at positions in good agreement with those one can expect for a two-dimensional lattice of hexagonally packed cylinders having a unit cell dimension $a = 398$ Å. This interaxial distance together with the polystyrene volume fraction, $\phi_{PS} = 0.19$, of the SIS-6-H polymer lead

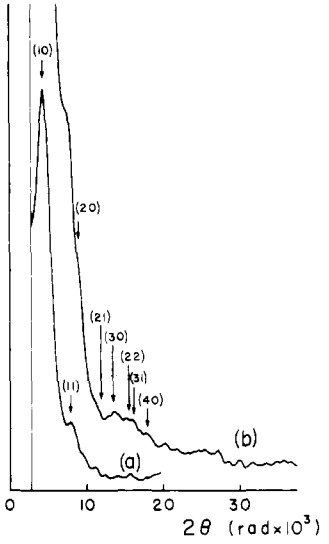

Figure 15. Small-angle X-ray scattering curve measured on SIS-6-H film cast from toluene. Exposure time: (a) 3 h, (b) 20 h. Arrows indicate the diffraction line positions calculated from eq 1 for a two-dimensional lattice of hexagonally packed cylinders of unit cell dimension $a = 398$ Å.

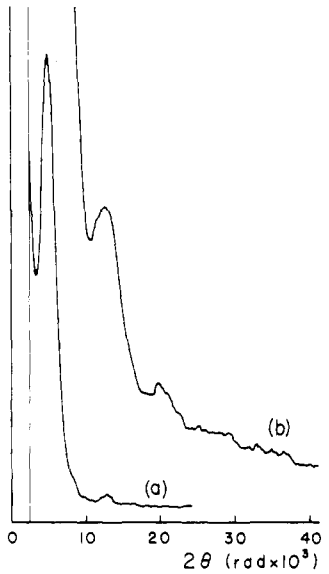

Figure 16. Small-angle X-ray scattering curve measured on a SIS-6-H film cast from cyclohexane. Exposure time: (a) 3 h, (b) 72 h.

to the value $R = 91$ Å for the radius of the polystyrene cylinders. This value is slightly higher than that obtained previously for the Kraton-G specimen cast from cyclohexane. This result was expected since the molecular weight of the polystyrene individual blocks in SIS-6-H is only 30% higher than that in Kraton-G.

In the case of the SIS-6-H specimen cast from cyclohexane, the scattering intensity curve (Figure 16) shows three peaks and, as for the Kraton-G specimen cast from heptane, it was observed that only the most intense peak at $2\theta = 5.0 \times 10^{-3}$ rad exhibits a definite shift upon stretching. Thus the second and third peaks arise from particle scattering from discrete spheres of polystyrene dispersed in a rubbery matrix. The value of the Bragg spacing calculated from the main peak position is 308 Å. As previously, this value can be assumed to correspond to the interdomain distance in the short-range ordered liquid-like lattice. Analysis of the second and third peaks in Figure 16 using the Rayleigh equation for scattering by independent spheres leads to the value $R = 113$ Å for the

radius of the polystyrene spheres. Here again this value is slightly higher than the value R = 110 Å one can calculate from the polystyrene volume fraction assuming a simple cubic arrangement.

Discussion

The above study performed on ABA block copolymers with polystyrene endblocks and with polyolefin midblocks indicates that the nature of the solvent used in the film preparation greatly influences the mechanical properties of the final materials. The changes observed in the mechanical properties are associated with a systematic change in the microdomain structures. Using a good solvent for the midblocks but either a poor or a nonsolvent for the polystyrene endblocks can result in specimens having mechanical behavior very close to that of unfilled vulcanized rubbers. The microdomain structures of these specimens are characterized as polystyrene discrete spheres dispersed in a rubbery matrix. For the sample having a low styrene content (SIS-6-H, w_S = 0.22), this structure was obtained by using a poor solvent for polystyrene (cyclohexane) while for the sample having a higher styrene content (Kraton-G, w_S = 0.29), a nonsolvent (heptane) was required. The main characteristics of the material so obtained are the absence of stress softening in the first extension cycle and a rubbery plateau over a wide range of temperatures. Dynamic thermomechanical measurements indicate that in the initial deformation process the load is essentially carried by the polyolefin phase. On the other hand, when the specimens are stretched to a strain ϵ = 1, SAXS measurements indicate a nearly affine deformation. This latter observation suggests that the internal strain is distributed uniformly within the rubbery matrix and that the polystyrene domains act mainly as a cross-linking agent without significant filler contribution, even though their volume fraction in the system may be as high as 0.25 (Kraton-G).

Increasing solvent affinity for polystyrene results in microdomain structures characterized as hexagonally packed cylinders of polystyrene. For the sample having a styrene content w_S = 0.29, this structure was obtained with cyclohexane which is still a poor solvent for polystyrene, while for the sample having styrene content w_S = 0.22 the same structure was obtained with toluene, a good solvent for polystyrene. Both materials show stress softening in the first extension but do not exhibit yield at low extension. Dynamic thermomechanical measurements indicate that in the initial deformation process a small fraction of the load is carried by the polystyrene phase. This suggests that the polystyrene cylinders are relatively short, but long enough to make a modest contribution to both tensile stress and storage modulus. Hence, it is likely that the stress softening effect observed at moderate extension ($0 < \epsilon < 3$) is associated with partial orientation of the short cylinders along the stretching direction.

The change of solvent from cyclohexane to toluene for the sample having styrene content w_S = 0.29 results in a change of microdomain structure from the hexagonally packed cylinders to the alternating lamellae. This change of structure has the most important effect on the mechanical properties. In the first extension the material shows a high initial Young's modulus, yield phenomenon at low elongation and neck propagation. Dynamical measurements indicate that before the yield phenomenon occurs the load is essentially carried by the polystyrene phase.

This suggests that the polystyrene lamellae are extended over longer regions than the cylinders. A better ordering of the two phases was also evidenced by the SAXS curve measured on toluene cast film which showed more intense diffraction peaks than cyclohexane cast film. Thus the initial behavior of the stress–strain curve measured on the toluene cast film can be explained by the breakdown and the orientation of the glassy lamellae in the first extension. This phenomenon is irreversible but leads to a material which shows again stress softening in the second extension. This indicates that when the load is removed, loose bonds reappear between the fragmented polystyrene domains.

The thermodynamic factors involved in microdomain formation for AB and ABA block copolymers have been studied by several authors.[20–25] The most important factors are the parent homopolymers incompatibility characterized by the interaction free energy parameter χ_{AB}, the interfacial free-energy contribution, the composition and the molecular weight of the block copolymers, and also the relative affinities of the casting solvent for the parent homopolymers. For cast films, it is admitted[20,21] that the organized structure observed in the solid material is strongly influenced by the micellar arrangements produced during the casting process. Thus the microdomain structure which forms during solvent evaporation can remain in the final material. This explains that different microdomain structures can be observed for a given block copolymer.

The present block copolymers have different polystyrene contents but have polystyrene endblocks of about the same molecular weights (1.0×10^4 for Kraton-G and 1.3×10^4 for SIS-6-H). Thus it is expected that the predominant factor which makes these copolymers behave differently during casting in a solvent is the larger polystyrene content for Kraton-G. On the other hand, the three solvents (heptane, cyclohexane, and toluene) which are all good solvents for the polyolefin midblocks present very different affinities for polystyrene. Heptane is a nonsolvent for polystyrene. In such a solvent it is expected that the micellar arrangement produced during solvent evaporation is characterized by spherical aggregates of polystyrene chains in a swollen matrix of polyolefin. Before the solvent content reaches the point where immobilization of the system occurs, the volume fraction of the swollen matrix is still sufficiently high for avoiding contacts between the polystyrene aggregates. This arrangement remains in the dry material and, as shown for Kraton-G, can be obtained for dry sample having a polystyrene volume fraction as high as 0.25.

Cyclohexane is a poor solvent for polystyrene. In such a solvent it is expected that the micellar arrangement produced during solvent evaporation involves both the polystyrene and the polyolefin swollen phases. However, the volume fraction of solvent located within the polystyrene microphases is expected to be much lower than that located within the polyolefin phase. This situation can lead to the same arrangement discussed before for heptane, but only for samples having a polystyrene content sufficiently low for avoiding contacts between the polystyrene swollen spherical domains. This appears to be the case for the SIS-6-H block copolymer whose polystyrene volume fraction in the dry state is 0.19. On the other hand, when the polystyrene content reaches a certain value between those of SIS-6-H and Kraton-G, the volume fraction of the dispersed swollen microphases is such that many spherical domains may connect together leading to cylindrical domains before immobilization of the system. The fact that cylindrical structures form and lamellar structures do not can be explained by the requirement to maintain a high interfacial area owing to the large difference of volume of the two swollen phases. Note that

the surface/volume ratio for cylinders of radius R is twice that of lamellae of thickness $2R$, but only $^2/_3$ that of the spheres of radius R.

Toluene is a good solvent for both polystyrene and the polyolefin midblocks in Kraton-G and SIS-6-H. Thus in this solvent it is expected that the polystyrene microphases are much more swollen than in cyclohexane. This results in a situation where the requirement for a high interfacial area is not as pronounced as in the case of cyclohexane. This requirement remains only for samples having low polystyrene contents, such as sample SIS-6-H. For samples having a higher styrene content, such as Kraton-G, the swollen system is such that lamellar structures are formed before immobilization of the system.

The present study offers examples in which a given ABA block copolymer shows two or three of the three fundamental types of microdomain structures (spherical, cylindrical, and lamellar) normally observed in block copolymer systems. Consequently, it is interesting to consider the relationship between the dimensions and the shapes of the polystyrene domains for each of the copolymers studied. On the other hand, comparison of the present data with similar data already published in literature for SBS and SI block copolymers reveals some trends worth noting. For the sake of the comparison, the domain sizes (radius R_S for spheres, radius R_C for cylinders, and thickness L for lamellae) divided by the unperturbed root-mean-square end-to-end distance, $(\overline{r_o^2})^{1/2}$, of a polystyrene chain of the same molecular weight as the individual polystyrene chains in the block copolymers will be used as structural characteristic ratios. The relation between root-mean-square end-to-end distance, $(\overline{r^2})^{1/2}$, for bulk polystyrene and molecular weight has been determined by Cotton et al.[26] using a neutron scattering technique. The result, $(\overline{r^2})^{1/2} = 0.67M^{1/2}$, is very close to the equivalent relation determined for polystyrene in θ solvent,[27] indicating that unperturbed dimensions also prevail in the bulk. From the SAXS results presented in the preceding section one obtains the following characteristic ratios for the Kraton-G specimens:

$$R_S/(\overline{r_o^2})^{1/2} = 1.45 \text{ for spheres}$$

$$R_C/(\overline{r_o^2})^{1/2} = 1.28 \text{ for cylinders}$$

$$L/(\overline{r_o^2})^{1/2} = 1.24 \text{ for lamellae}$$

and the following ones for the SIS-6-H specimens:

$$R_S/(\overline{r_o^2})^{1/2} = 1.48 \text{ for spheres}$$

$$R_C/(\overline{r_o^2})^{1/2} = 1.19 \text{ for cylinders}$$

Interestingly, a survey of the literature data indicates that values of $R_S/(\overline{r_o^2})^{1/2}$ in the range 1.46 to 1.73 can be computed for spherical polystyrene microdomains from SAXS results obtained for five different SBS copolymers[15,17] having styrene weight fractions, w_S, in the range 0.22 to 0.30 and polystyrene endblock molecular weights, M_{PS}, in the range 1×10^4 to 14×10^4. Note that no evident correlation can be seen between the ratios $R_S/(\overline{r_o^2})^{1/2}$ and molecular weights M_{PS}. On the other hand, the value $R_S/(\overline{r_o^2})^{1/2} = 1.64$ can be computed from data obtained for a SI copolymer[16] having a styrene weight fraction $w_S = 0.18$ and $M_{PS} = 5.1 \times 10^4$. Averaging the six values of $R_S/(\overline{r_o^2})^{1/2}$ computed from the literature data together with the two values computed from the present data yields $R_S/(\overline{r_o^2})^{1/2} = 1.6 \pm 0.1$ as a characteristic ratio for spherical polystyrene microdomains in systems where $0.18 \leq w_S \leq 0.30$.

In the cases where cylindrical polystyrene microdomains have been observed, literature data for two SBS copolymers[28,29] ($w_S = 0.25$ and 0.29, $M_{PS} = 1.0 \times 10^4$ and 1.4×10^4, respectively) lead to the same value, $R_C/(\overline{r_o^2})^{1/2} = 1.12$, while data for two SI copolymers[30] ($w_S = 0.25$, $M_{PS} = 1.2 \times 10^4$ and 2.4×10^4, respectively) lead to values $R_C/(\overline{r_o^2})^{1/2} = 1.24$ and 1.28, respectively. Averaging these four literature results together again with the present work results, one obtains $R_C/(\overline{r_o^2})^{1/2} = 1.2 \pm 0.1$ as a characteristic ratio for cylindrical polystyrene microdomains in systems where $0.22 \leq w_S \leq 0.29$.

Finally, in the cases where lamellar structures have been observed in the literature, it turns out that an average value $L/(\overline{r_o^2})^{1/2} = 1.63 \pm 0.15$ can be computed from data published on two SBS copolymers[29,31] and two SI copolymers[32,33] having styrene weight fractions, w_S, in the range 0.44 to 0.59 and M_{PS} in the range 1.4×10^4 to 6.2×10^4. The value $L/(\overline{r_o^2})^{1/2} = 1.23$ computed from the Kraton-G data departs considerably from the average value of 1.63 obtained for the SBS and SI copolymers. As it will be shown below, this departure can be explained by the difference in styrene content between Kraton-G ($w_S = 0.29$) and the SBS and SI copolymers ($0.44 < w_S < 0.60$) studied in the literature.

With the above results concerning the relationships between $R/(\overline{r_o^2})^{1/2}$ (or $L/(\overline{r_o^2})^{1/2}$) and the microdomain morphologies it was interesting to test, at least to a certain extent, the theoretical models which have been proposed in the literature for predicting the morphological behavior of block copolymers. We have chosen to test the model proposed by Meier,[20] since this model allows quantitative predictions of the characteristic ratios $R/(\overline{r_o^2})^{1/2}$ (or $L/(\overline{r_o^2})^{1/2}$) in terms of both the microdomain morphology and the block copolymer composition. According to Meier's model, the physical factors which govern the microdomain sizes in AB and ABA block copolymers are the finite lengths of the A and B chains and the requirement that space in the individual microphases be uniformly filled with polymer segments of one type only. Meier's calculations based on the diffusion equation led to the following expressions for the sizes of the discrete A domains in terms of the unperturbed root-mean-square end-to-end distance, $(\overline{r_o^2})^{1/2}$, of the chains A:

$$R_S \simeq 1.33\alpha_S(\overline{r_o^2})^{1/2} \tag{3}$$

$$R_C \simeq 1.0\alpha_C(\overline{r_o^2})^{1/2} \tag{4}$$

and

$$L \simeq 1.4\alpha_L(\overline{r_o^2})^{1/2} \tag{5}$$

In these equations, α is the linear chain expansion characterizing the chain perturbation due to the space-filling forces. As shown by Meier,[20] for a given microdomain structure, the expansion factor of chains A, α_A, must be related to that of chains B, α_B. Relations between α_A and α_B have been derived by Meier for AB block copolymers whose chains A and B have the same unperturbed effective segmental length. They are the following:[20]

$$\alpha_A/\alpha_B \simeq (M_A/M_B)^{1/2} \text{ for lamellae} \tag{6}$$

$$\alpha_A/\alpha_B \simeq (M_A/M_B)^{1/6} \text{ for cylinders} \tag{7}$$

and

$$\alpha_A \simeq \alpha_B \text{ for spheres} \tag{8}$$

In these relations, M_A and M_B are the molecular weights of chains A and B, respectively. Equations 6–8 predict that the characteristic ratio $L/(\overline{r_o^2})^{1/2}$ for lamellar structures is much more dependent upon the copolymer composition than those for cylindrical and spherical structures. Note that eq 6–8 have been derived from packing considerations alone. For that reason, they are not strictly adequate for ABA block copolymers since the expansion factor, α_B, of the midblock B can be changed by the additional constraints due to the physical requirement that both ends of the midblock must be anchored to domains A. Nevertheless, the experimental results presented above for the characteristic ratios $L/(\overline{r_o^2})^{1/2}$ of polystyrene lamellae in various ABA and AB block copolymers of different compositions indicate that α_{PS}, according to eq 5, increases from about 0.9 to about 1.2 when styrene weight fraction, w_S, increases from 0.3 to 0.6. Such a dependence, i.e., increase of α_{PS} with increase of w_S, is predicted by Meier's model, indicating that the space-filling forces are the predominant factor which governs chain expansion in lamellar structures.

Spherical and cylindrical polystyrene structures have been observed only for a narrow range of copolymer compositions. For that reason, the experimental data available cannot provide information concerning the variation of α_{PS} with copolymer composition. However, in the range of compositions where data are available, i.e., $0.18 \leq w_S \leq 0.30$, the use of eq 3 and 4 with $R_S/(\overline{r_o^2})^{1/2} = 1.6 \pm 0.1$ for spheres and $R_C/(\overline{r_o^2})^{1/2} = 1.2 \pm 0.1$ for cylinders, respectively, yields $\alpha_{PS} = 1.2 \pm 0.1$ for both types of structure. In the same range of compositions, Kraton-G data yield $\alpha_{PS} = 0.9$ for lamellar structure. According to these results, for systems having polystyrene weight fractions w_S close to 0.3, the chain conformations in both spherical and cylindrical domains would be more extended than in the bulk while those in lamellar domains would be less extended than in the bulk. Such a difference of behavior between lamellar and spherical or cylindrical structures was expected since the thickness of the lamellae is only slightly greater than $(\overline{r_o^2})^{1/2}$ while the diameters of the spheres or cylinders are more than twice $(\overline{r_o^2})^{1/2}$.

Acknowledgment. This work was supported by the National Research Council of Canada and the Quebec Ministry of Education. The authors wish to express their appreciation to Dr. T. L. Keelen of the Shell Development Co. for the supply of the Kraton GX-6500 sample. The authors also wish to thank the Canadian 220-MHz NMR Center for making the ^1H NMR measurements.

References and Notes

(1) A. Laramée, P. Goursot, and J. Prud'homme, *Makromol. Chem.*, **176**, 3079 (1975).
(2) J. F. Beecher, L. Marker, R. D. Bradford, and S. L. Aggarwal, *J. Polym. Sci., Part C*, **26**, 117 (1969).
(3) G. S. Fielding-Russel, *Rubber Chem. Technol.*, **45**, 252 (1972).
(4) S. Bagrodia and G. L. Wilkes, *J. Biomed. Mater. Res.*, **10**, 101 (1976).
(5) A. Beamish, R. A. Goldberg, and D. J. Hourston, *Polymer*, **18**, 49 (1977).
(6) S. Ayano and S. Yabe, *Polym. J.*, **1**, 706 (1970).
(7) N. H. Canter, *J. Polym. Sci., Part A-2*, **6**, 155 (1968).
(8) M. Morton, J. E. McGrath, and P. C. Juliano, *J. Polym. Sci., Part C*, **26**, 99 (1969).
(9) E. Pedemonte, A. Turturro, and G. Dondero, *Br. Polym. J.*, **6**, 277 (1974).
(10) P. J. Flory, "Principles of Polymer Chemistry", Cornell University Press, Ithaca, N.Y., 1953, Chapter XI.
(11) J. J. Aklonis, W. J. MacKnight, and M. Shen, "Introduction to Polymer Viscoelasticity", Wiley-Interscience, New York, N.Y., 1972.
(12) G. Kraus, K. W. Rollmann, and J. O. Gardner, *J. Polym. Sci., Polym. Phys. Ed.*, **10**, 2061 (1972).
(13) A. E. Skoulios in "Block and Graft Copolymers", J. J. Burke and V. Weiss, Ed., Syracuse University Press, Syracuse, N.Y., 1973, p 121.
(14) G. Oster and D. P. Riley, *Acta Crystallogr.*, **5**, 272 (1952).
(15) P. R. Lewis and C. Price, *Polymer*, **12**, 258 (1971).
(16) T. Inoue, M. Moritani, T. Hashimoto, and H. Kawai, *Macromolecules*, **4**, 500 (1971).
(17) E. Campos-Lopez, D. McIntyre, and L. J. Fetters, *Macromolecules*, **6**, 415 (1973).
(18) G. Oster and D. P. Riley, *Acta Crystallogr.*, **5**, 1 (1952).
(19) A. Guinier, "X-Ray Diffraction", W. H. Freeman, San Francisco, Calif., 1963, p 323.
(20) D. J. Meier in "Block and Graft Copolymers", J. J. Burke and W. Weiss, Ed., Syracuse University Press, Syracuse, N.Y., 1973, p 105.
(21) H. Kawai, T. Soen, T. Inoue, T. Ono, and T. Uchida, *Mem. Fac. Eng., Kyoto Univ.*, **33**, 383 (1971).
(22) U. Bianchi, E. Pedemonte, and A. Turturro, *Polymer*, **11**, 268 (1970).
(23) S. Krause, *Macromolecules*, **3**, 84 (1970).
(24) D. F. Leary and M. C. Williams, *J. Polym. Sci., Polym. Phys. Ed.*, **11**, 345 (1973).
(25) E. Helfand, *Macromolecules*, **8**, 552 (1975).
(26) J. P. Cotton, D. Decker, H. Benoit, B. Farnoux, H. Higgins, G. Jannink, R. Ober, C. Picot, and J. Des Cloiseaux, *Macromolecules*, **7**, 863 (1974).
(27) G. C. Berry, *J. Chem. Phys.*, **44**, 4550 (1966).
(28) A. Keller, J. Dlugosz, M. J. Folkes, E. Pedemonte, F. P. Scalisi, and F. M. Willmouth, *J. Phys. (Paris)*, **32**, C5a-295 (1971).
(29) W. R. Krigbaum, S. Yazgan, and W. R. Tolbert, *J. Polym. Sci., Polym. Phys. Ed.*, **11**, 511 (1973).
(30) C. Price, T. P. Lally, A. G. Watson, D. Woods, and M. T. Chow, *Br. Polym. J.*, **4**, 413 (1972).
(31) J. Dlugosz, M. J. Folkes, and A. Keller, *J. Polym. Sci., Polym. Phys. Ed.*, **11**, 929 (1973).
(32) T. Hashimoto, K. Nagatoshi, A. Todo, H. Hasegawa, and H. Kawai, *Macromolecules*, **7**, 364 (1974).
(33) B. Ptaszynski, J. Terrisse, and A. Skoulios, *Macromol. Chem.*, **176**, 3483 (1975).